Mechanical Systems and Signal Processing 81 (2016) 88–107

Contents lists available at ScienceDirect

Mechanical Systems and Signal Processing

journal homepage: www.elsevier.com/locate/ymssp

A comparative study between Empirical Wavelet Transforms and Empirical Mode Decomposition Methods: Application to bearing defect diagnosis

M. Kedadouche, M. Thomas *, A. Tahan

Department of Mechanical Engineering, École de Technologie Supérieure, Montréal, QC, Canada H3C 1K3

ARTICLE INFO

Article history:
Received 21 May 2014
Received in revised form
17 February 2016
Accepted 24 February 2016
Available online 16 March 2016

Keywords:
Bearing fault
Acoustic emission
Empirical Mode Decomposition (EMD)
Ensemble Empirical Mode Decomposition (EEMD)
Empirical Wavelet Transform (EWT)

ABSTRACT

The Ensemble Empirical Mode Decomposition (EEMD) is a noise assisted method that may sometimes provide a significant improvement on Empirical Mode Decomposition (EMD). However, the amplitude and number of added noise need to be selected when applying the EEMD method. Furthermore, the computation time which depends on the number of ensemble trails is very high compared to the EMD. In this paper, a new way for choosing the appropriate added noise is presented. Conversely, a recently-developed method called the Empirical Wavelet Transform (EWT) is investigated. A comparative study between the EMD and EWT methods is conducted. The results show that the EWT is better than the EEMD and EMD on mode estimates and computation time is significantly reduced. An experimental study on bearing diagnosis is conducted. The EWT is applied to experimental data coming from damaged bearings. In the paper, an index selection is introduced that allows for the automatic selection of the Intrinsic Mode Functions (IMF) that should be used to perform the envelope spectrum. It is shown that choosing all the IMF selected by the index is more efficient than only choosing the best one. The envelope of the sum of the selected IMF clearly reveals the bearing frequencies and its harmonics which are excited by the defect. This approach seems to be an effective and efficient method for processing bearing fault signals.

1. Introduction

The bearing may be considered one of the most stressed parts in rotating machines. Early stage bearing defects first excite the resonance frequencies which manifest in the high frequency domain. The traditional fault diagnosis techniques mainly contain demodulations and envelope-based methods due to their ability to identify defect-induced frequency in the bearing. However, the major challenge in the application of this technique is the proper selection of the center frequency and bandwidth to perform the envelope spectrum.

Recently, signal processing techniques for non-stationary and noisy signals has attracted considerable attention. One of them is the Empirical Mode Decomposition (EMD). EMD is a self-adaptive algorithm and is suitable for analyzing the non-stationary and nonlinear phenomena, since it can adaptively decompose the signal into Intrinsic Mode Functions (IMFs) [1,2]. The basic idea is to decompose the signal into multiple IMFs and then select the appropriate IMF to construct the envelope spectrum using the Hilbert transform. Lei et al. [3] present a good review of EMD applied to a fault diagnosis in

* Corresponding author.
E-mail addresses: mourad.kedadouche@hotmail.fr (M. Kedadouche), marc.thomas@etsmtl.ca (M. Thomas), antoine.tahan@etsmtl.ca (A. Tahan).

http://dx.doi.org/10.1016/j.ymssp.2016.02.049
0888-3270/

rotating machinery. However, it is well known that EMD suffers from a major drawback which is mode mixing [4]. To overcome this drawback, an Ensemble EMD (EEMD) is proposed [5]. The method proposed is to add some white noise with limited amplitude to the researched signals. Therefore, the EEMD method is considered as a significant improvement over the EMD method, and is recommended as a substitute for the EMD method. Indeed, the EEMD method has shown its superiority over the EMD method in many applications, and EEMD has been widely applied in fault diagnosis of rotating machinery, such as in gear fault diagnosis [6,7], rolling bearing fault diagnosis [8–10,13] and rotor fault diagnosis [11]. However, there is a lack on how to choose the appropriate amplitude of the added noise and its computation efficiency is fairly low.

Recently, a new method called "Empirical Wavelet Transform" (EWT) was developed by Gilles [12]. The concept is based on wavelet decomposition. The main idea is to extract the modes of a signal by designing an appropriate wavelet filter bank. EWT is used in this paper to diagnose bearing defects and its effectiveness is compared to that of EMD. EWT decomposition is based on segmentation of the Fourier spectrum. With bearing defects, unfortunately, segmentation can be affected by interference components, and substantial noise and modulation effects. Thirumala [36] applied EWT to the electrical signal and proposed another way to estimate the support boundaries of the filter bank. He used a threshold magnitude set to 3% of the fundamental magnitude to recognize the significant frequencies; whereas, the threshold for frequency distance was 8 Hz to avoid overestimation of false frequencies. In this paper, in order to overcome this drawback, a new methodology for spectrum segmentation is proposed. First, the performance of the proposed method is compared to the EMD and EEMD method. Secondly, an automatic selection of the component excited by the defect is proposed to perform the envelope spectrum.

In this paper, the authors propose to use the Empirical Wavelet Transform to diagnose bearing defects and compare its efficiency with an improved EEMD. This paper is organized as follows. Section 2 provides a theoretical background of EMD, EEMD and EWT. In this section, an improvement of EEMD is proposed. In Section 3, a comparison between the improved EEMD, EMD and EWT is presented through simulated signals from bearing defect. An application of EWT to experimental data acquired from damaged bearings via acoustic emission is presented. A new way to select the IMF related to the defect to accomplish a good diagnosis will take place. Finally, conclusions are drawn in Section 4.

2. Theoretical background

2.1. Empirical Mode Decomposition (EMD)

The EMD method can self-adaptively decompose a non-stationary signal into a set of intrinsic mode functions (IMFs) from high frequencies to low frequencies. The decomposed signal may be written as:

$$x(t) = \sum_{i=1}^{N} C_i(t) + r_N(t) \tag{1}$$

Where $C_i(t)$ indicates the $i^{th}IMF$and $r_N(t)$ represents the residual of the signal $x(t)$.

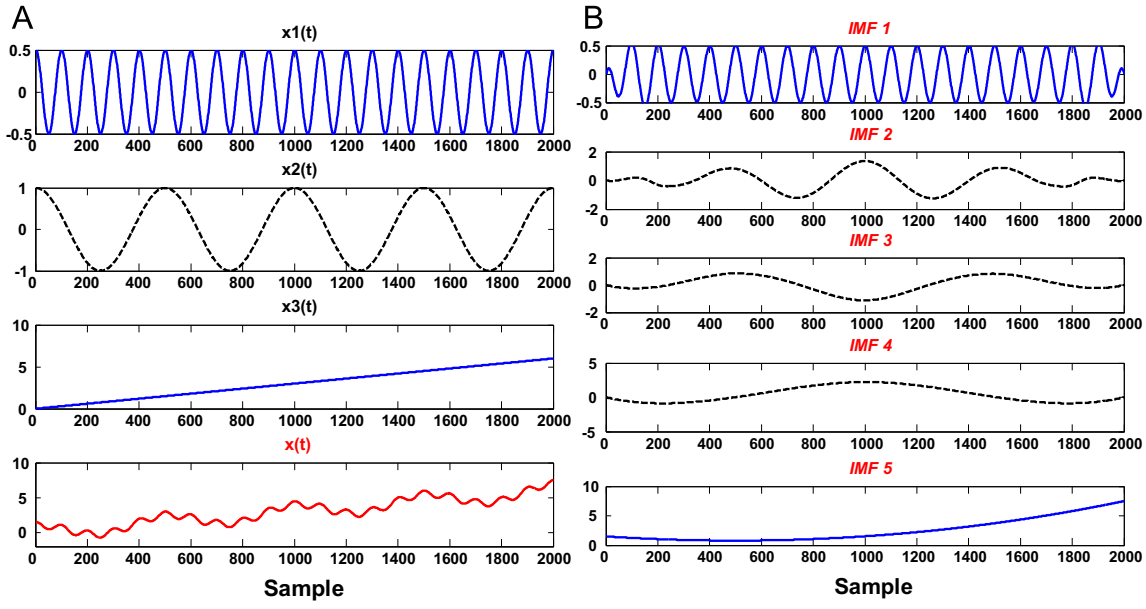

Fig. 1. (A) The simulated signal $x(t)$ (red color) and its components (blue and black color) and (B) the EMD decomposition of the signal $x(t)$.(For interpretation of the references to color in this figure legend, the reader is referred to the web version of this article.)

Each *IMF* function respects the following conditions:

(1) The number of extrema and the number of zero crossings must either equal or differ, at most, by one;
(2) The value of the moving average envelope defined by local maxima and the envelope defined by local minima are zero.

2.1.1. Mode mixing

EMD is well known and widely used. However, it suffers from the major drawback of mode mixing. Mode mixing is defined as a single IMF including a component of a similar scale residing in different IMFs [14]. As discussed in [4], the intermittence may not only cause serious aliasing in the time–frequency distribution, but also makes the physical meaning of individual IMF unclear. To illustrate the problem of mode mixing in EMD, a simulated signal used in [15] given by Eq. (2) is considered:

$$x(t) = x_1(t) + x_2(t) + x_3(t) \tag{2}$$

where

$$\begin{cases} x_1(t) = 0.5\ \cos(40\pi t) \\ x_2(t) = \ \cos(8\pi t) \\ x_3(t) = 6t \end{cases} \tag{3}$$

The simulated signal, shown in Fig. 1(A) (red color), is made with the sum of three distinct components given by Eq. (3). Performing an EMD algorithm as developed by [16] on the signal, five IMFs are obtained and shown in Fig. 1(B). It is clear that the four *IMFs* are distorted. Mode mixing is occurring between IMF_2, IMF_3 and IMF_4. The sinusoidal wave $x_2(t)$ is decomposed into three IMFs (IMF_2, IMF_3 and IMF_4). This is a typical problem in mode mixing.

2.2. Ensemble Empirical Mode Decomposition (EEMD)

To overcome the mode mixing separation problem, a new noise assisted data analysis method is proposed by Wu and Huang [4]. The EEMD defines the true *IMF*components as the mean of an ensemble of trials, each consisting of the signal plus a white noise of finite amplitude. The proposed EEMD is defined as follows:

(1) Add a white noise series to the targeted data $x(t)$
(2) Decompose the data $x(t)$ with added white noise into *IMFs*.
(3) Repeat step 1 and step 2 a multitude of times, with different white noise series at each time.
(4) Obtain the (ensemble) means of corresponding *IMFs* of the decompositions as the final result (Eq.(4)).

$$y_n = \frac{1}{M}\sum_{m=1}^{M} c_{n,m} \tag{4}$$

where y_n represent the mean of M trials for each IMF_n.

2.2.1. Review of the EEMD parameter selection

The critical parameters that directly affect the performance of the EEMD method are: the amplitude of the added white noise and the ensemble number needed. Lei et al. [17–19] and Zhou et al. [20] stated that there were no specific equations reported in the literature to guide the choice of EEMD parameters, especially noise amplitude. In most of cases, they tried different noise amplitudes and selected from them. Wu and Huang [4] provided a relationship among the ensemble number N_E, the amplitude of the added white noise $\langle a \rangle$ and the standard deviation of error $\langle e \rangle$ by using the equation:

$$\ln(e) + \frac{a}{2}\ln(N_E) = 0 \tag{5}$$

They suggested that the amplitude of the added white noise is approximately ≈ 0.2 of a standard deviation of the original signal and the value of an ensemble is a few hundred. However, this is not always applicable for signals in various applications.

Guo et al. [21] provided a strategy to determine parameter settings of the EEMD method:

(1) When the signal is dominated by the high-frequency signal component, the high-frequency component is more easily separated from the low-frequency signal component and the lower noise amplitude is able to separate the mixed modes. If the peak value of the high-frequency component is higher, the noise amplitude should be increased appropriately. When the signal is dominated by low-frequency signal components, the noise amplitude should be larger.
(2) Once the noise amplitude is determined, when not considering the computation cost, a larger value for the ensemble number will lead to smaller errors which are mainly caused by the added white noise, especially for high-frequency

signal components. To some degree, continuing to increase the ensemble number will result in only a minor change in errors.

Zvokelj et al. [22,23], Chang and Liu [24], Zhang et al. [25], and Yeh et al. [26] independently introduced the signal-to-noise ratio (SNR) as a performance index to select the noise amplitude. The assumption of their methods relies on the a priori knowledge of the analyzed signal or its power. Niazy et al. [27] used relative root-mean-square error (*RMSE*) given by Eq. (6) to evaluate the performances of EEMD when trying different levels of added white noise. The RMSE is defined as the ratio between the root-mean-square of the error and the root-mean-square of the original signal, where the error is the difference between the original signal $x_0(k)$, and the selected $IMF(c_{max}(k))$ having the highest correlation with the original signal and containing its main signal component.

$$RMSE = \sqrt{\frac{\sum_{k=1}^{n}(x_0(k)-c_{max}(k))^2}{\sum_{k=1}^{n}(x_0(k))}} \tag{6}$$

However, they did not provide guidance on how to select appropriate noise levels. Wei et al. [28] propose a modified equation as shown in Eq. (7) to compute the amplitude of the white noise needed to perform the EEMD method.

$$RMSE_{Modified} = \sqrt{\frac{\sum_{k=1}^{n}(x_0(k)-c_{max}(k))^2}{\sum_{k=1}^{n}(x_0(k)-\overline{x_0})}} \tag{7}$$

2.2.2. A new method for improved EEMD

Mode mixing is defined as a single *IMF* which includes a component of a similar scale residing in different*IMFs*. This means that the correlation between these *IMF*is strong. Initially, the correlation between the component $x_1(t)\&x_2(t)$ and $x_2(t)\&x_3(t)$is close to zero. The coefficients are given in Table 1.

We propose to choose the amplitude white noise that assures the lowest coefficient correlation between two successive*IMF*. The Pearson coefficient of correlation between successive *IMF* is given by Eq. (8)

$$r(k) = \frac{\sum_{i=1}^{N}(IMF_k(i)-\overline{IMF}_k)(IMF_{k+1}(i)-\overline{IMF}_{k+1})}{\sqrt{\sum_{i=1}^{N}(IMF_k(i)-\overline{IMF}_k)^2}\sqrt{\sum_{i=1}^{N}(IMF_{k+1}(i)-\overline{IMF}_{k+1})^2}} \tag{8}$$

where N is length of the signal and k is $i^{th}IMF$.

In the considered example, the simulated signal presents three components. Therefore, it is necessary to note the number of the estimated components by the EEMD method for each added white noise. The simulation is conducted for different amplitude white noise $\langle a\rangle$ given by the relation:

$$a = L\,\sigma_x \tag{9}$$

where σ_x is standard deviation of the signal $x(t)$ and L is the level needed to perform the EEMD.

Generally, an ensemble number N_E of a few hundred averages will lead to an exact result. The remaining noise would cause an error less than a fraction of one percent if the added noise amplitude is a fraction of the standard deviation of the investigated signal [4]. The simulation experiment is conducted with $N_E = 100$. Fig. 2 shows the variation of coefficients of correlation for different levels $\langle L\rangle$. It is noted that the lowest coefficients of correlation are given for $L \leq 6.10^{-5}$and at this level, the number of *IMF*computed is equal to 3 which is the expected component number. For $L \geq 6.10^{-5}$, we note some regions when the correlation coefficient is close to zero, but at this stage, the EEMD overestimates the number of *IMF*. The appropriate limit amplitude of the added noise is thus equal to $6.10^{-5}\sigma_x$. Fig. 3(A) presents the decomposition EEMD of the signal using the selected amplitude noise ($6.10^{-5}\sigma_x$) and Fig. 3(B) presents the decomposition EEMD with the amplitude of added noise equal to $0.2\,\sigma_x$.

It is noted that the performance of EEMD is better with our parameters (Fig. 3(A)). With the standard method (Fig. 3(B)), the EEMD over estimate the number of components and we observe that the four first $IMF_{(1-4)}$ are only noises caused by the high value of the added noise.

2.3. Empirical Wavelet Transforms (EWT)

The Empirical Wavelet Transform developed by Gilles [12] presents a new approach for building adaptive wavelets. The main idea is to extract the different signal modes by designing an appropriate wavelet filter bank adapted to the processed

Table 1
Coefficient of correlation between the components of $x(t)$

	Coefficient of correlation
$x_1(t)\&x_2(t)$	9.9850e-004 ≈ 0
$x_2(t)\&x_3(t)$	7.6050e-018 ≈ 0

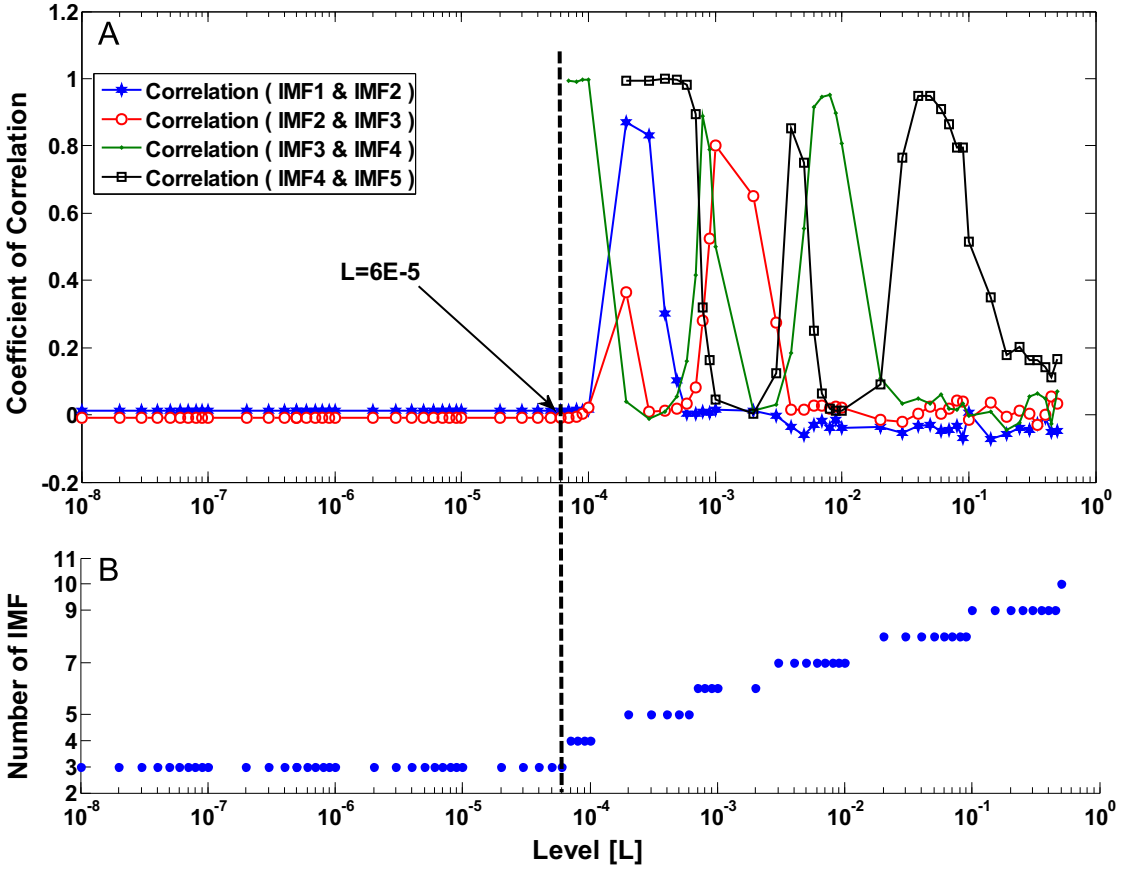

Fig. 2. The correlation coefficient between successive *IMF*and the number of the *IMF* computed by EEMD of the simulated signal $x(t)$.

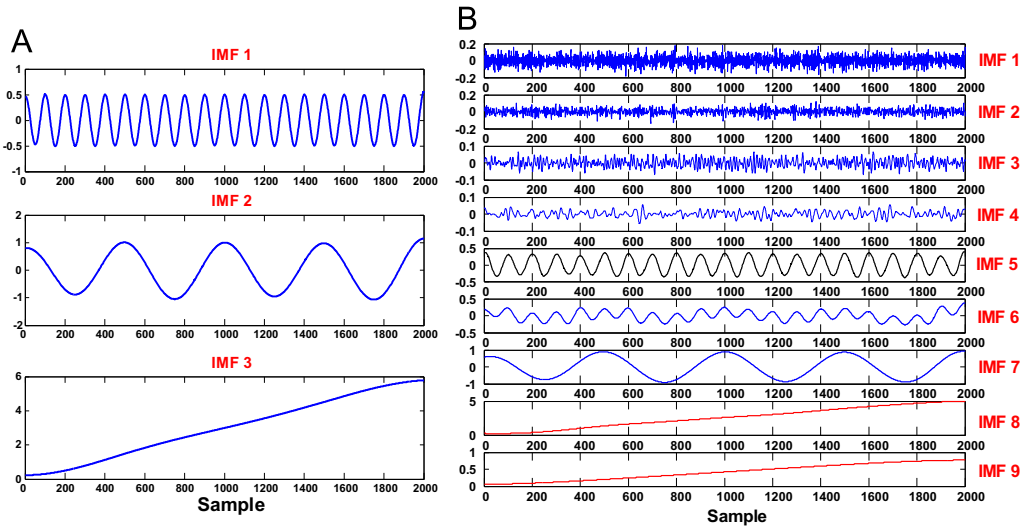

Fig. 3. (A) The EEMD decomposition of $x(t)$ using the added noise estimated by our approach and (B) the EEMD decomposition of the signal $x(t)$with the amplitude of the added noise equal to 0.2 σ_x.

signal. Considering the Fourier point of view, this construction is equivalent to building set of band pass filters. One way to reach the adaptability is to consider that the filters' supports depend on where the information is located in the spectrum of the analyzed signal. The wavelet transform is obtained by computing the inner products $w_x(u,s)=\langle x,\varphi_{u,s}\rangle$ where $\varphi_{u,s}$ is given by Eq. (10). A useful property of the EWT is that it can be viewed as the application of a filter bank decomposition of

the Fourier line (each filter is corresponding to one scale). In practice, the most used case is the dyadic case, $s=2^j$

$$\varphi_{u,s}(t)=\frac{1}{\sqrt{s}}\varphi\left(\frac{t-u}{s}\right) \tag{10}$$

However, this decomposition does not necessarily correspond to "modes" positions. The idea is to combine the strength of a wavelet's formalism with the adaptability of the EMD. Gilles [12] proposes to segment the Fourier spectrum. The aim is to separate different portions of the spectrum which correspond to modes centered on a specific frequency. The concept is to find the local maxima of the spectrum signal and take support boundaries as the middle between successive maxima.

The empirical mode is given by (Eqs. (11) and 12). The EWT can be defined in a similar way as the normal wavelet transform. The details coefficients are obtained by the inner product of applied signal, with the empirical scaling function as given:

$$IMF_{n=1:N-1}=W_x(n,t)=\langle x(t),\hat{\varphi}_n\rangle=IFFT\left(X(w)\times\hat{\varphi}_n(w)\right) \tag{11}$$

The approximation coefficients are given by the inner product with the scaling function:

$$IMF_N=W_x(1,t)=\left\langle x(t),\hat{\phi}_1\right\rangle=IFFT\left(X(w)\times\hat{\phi}_1(w)\right) \tag{12}$$

where, $\hat{\phi}_1(w)$ is the scaling function and $\hat{\varphi}_n(w)$ is the empirical wavelet.

More details about the construction of the filter bank are given in the Appendix. The performance of EWT depends on the number N which is the expected number of the filter bank. For a simulated signal as given in Eq. (2), the number N s equal to the number of the simulated components ($N=3$). Fig. 4(A) shows the Fourier partitioning of the empirical filter bank. $\hat{\phi}_1(w)$ is the scaling function and $\hat{\varphi}_n(w)$ ($n=1..2$) is the empirical wavelet. The decomposition EWT applied to $x(t)$ is shown in Fig. 4 (B). It is clear that EWT is able to detect the presence of modes in the spectrum and provides different components which are close to the original ones. However, the EMD always overestimates the number of modes (see Fig. 2) and then separate some information which is, originally, part of the same component. EEMD gives the same results than EWT. The difficulties are in choosing the right white noise and the ensemble number N_E needed.

Fig. 5B shows the computation time required to execute the three algorithms (EMD, EEMD and EWT). The computer used is an HP Compaq with an AMD Phenom™ 9600 B Quard-Qore processor 2.3 GHz and 4 Gb memory, running Windows 7, 64-bit and MATLAB R2011b. We can observe that EWT can reduce the time by 95.96%, as compared with the EMD method, and by 98.91%, as compared with the EEMD method. This indicates that the EWT method is an effective and efficient method. The flow chart of the algorithm of EWT is given in Fig.5(A).

The performance of EWT depends on the number N of components which is the number of filter banks introduced at the beginning of the algorithm (see Fig. 5(A)). In experimental analysis, this number is unknown since no a priori information is available. In such cases, it would be interesting to estimate the appropriate number of modes. In the case of damaged bearings, the defects at an early stage excite the resonance frequencies. Those resonances correspond to the bearing modes. Therefore, an Experimental Modal Analysis to estimate the number of frequency resonance can be used or an idea of the number of modes from a spectral analysis can be provided.

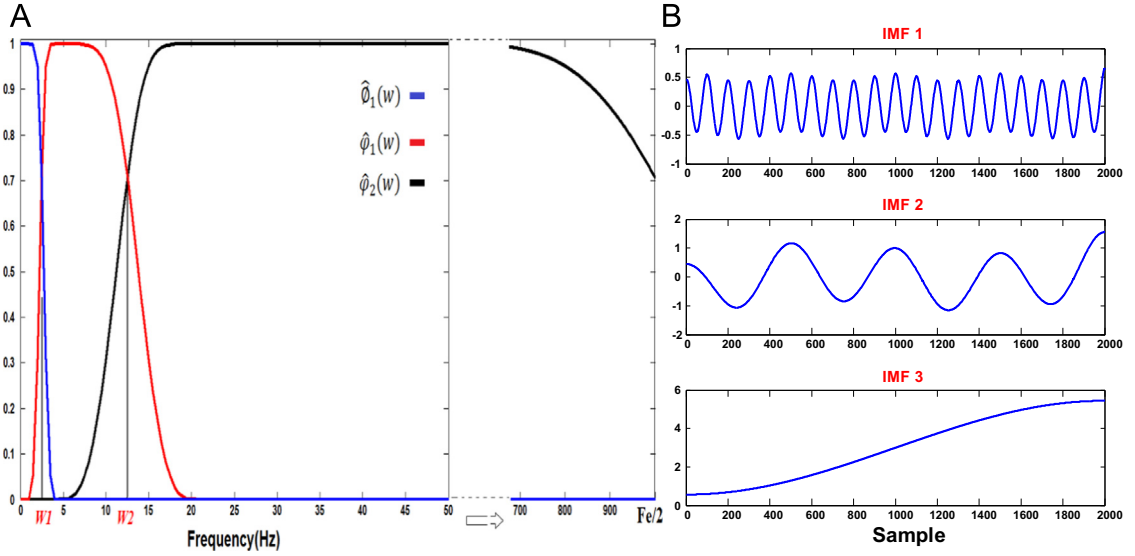

Fig. 4. (A) Fourier partitioning of the empirical filter bank. $\hat{\phi}_1(w)$Scaling function, $\hat{\varphi}_n(w)$ ($n=1..2$) Empirical Wavelet and (B) the decomposition EWT.

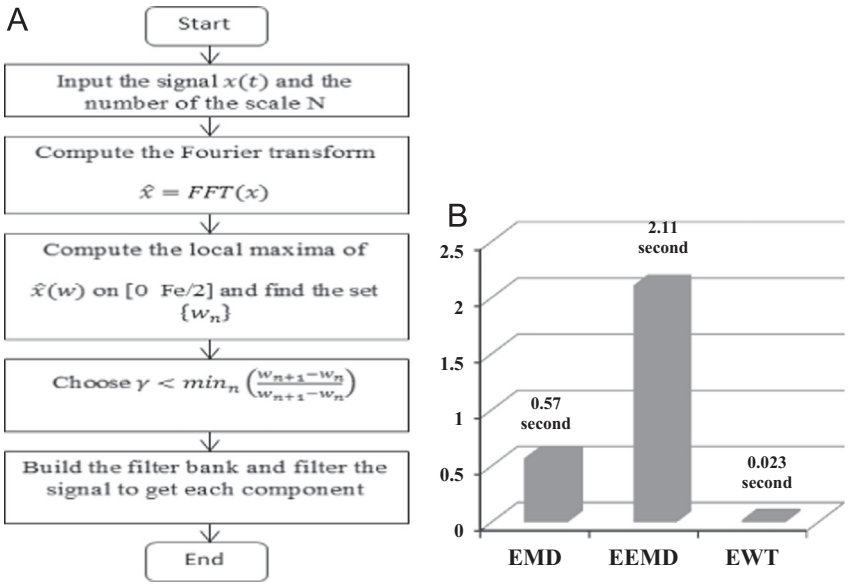

Fig. 5. (A) The flow chart of the EWT method and (B) comparisons of computing time between the three different methods.

Table 2
Values of $f_i(Hz)$and α_i

$\ll i \gg$	f_i(Hz)	α_i
1	500	100
2	2500	500
3	4000	300

3. Bearing faults diagnosis based on EWT and EEMD

3.1. Simulated signal

The numerical simulated signal that has been chosen is similar to the signal used in [29] with added noise. Its mathematic formulation is given as:

$$x(t) = A_i e^{-\alpha_i t'} \sin(2\pi f_i t) + 0.2 \sin(2\pi F_r t) + 0.1 \sin(2\pi(2F_r)t) + n(t) \tag{13}$$

$$t' = mod\left(t, \frac{1}{F_m}\right) \tag{14}$$

where «*mod*» is a Matlab function which returns the modulus after division, and

$$n(t) \sim N(0, 0.1) \tag{15}$$

where $n(t)$ is a Gaussian distributed random signal with 0 mean and standard deviation of 0.1.

The three frequency resonances chosen and the $\langle \alpha_i \rangle$ are listed in Table 2. The F_m is the bearing fault frequency (BPFO equal to 50 Hz). And F_s is the sampling frequency set to 12,500 Hz. $F_r = 20$ Hz is the frequency rotation and $2F_r = 40$ Hz is the first harmonic. A normally distributed random signal ($n(t)$) with 0 mean and standard deviation of 0.1 is added into the simulated signal in Eq. (13). The corresponding signal $x(t)$ is shown in Fig. 6.

3.1.1. Application of EMD and EEMD

The result of EMD is shown in Fig. 7. It exhibits 18 components. Some meaningless false components are also obtained. To overcome this drawback, EEMD is applied to the signal.

Before performing EEMD, the amplitude of the added white noise is estimated using the coefficients of correlation. Fig. 8 shows the variation of coefficients of correlation between successive *IMF*. The selected level limit is $L = 2.10^{-5}$ and the number of *IMF* is estimated to 10. For other values, an over estimation in the number of *IMF* and/or a higher coefficient correlation is observed. Performing EEMD for a signal $x(t)$ with these parameters ($L = 2.10^{-5}$ and $N_E = 100$), the decomposition is given in Fig. 9.

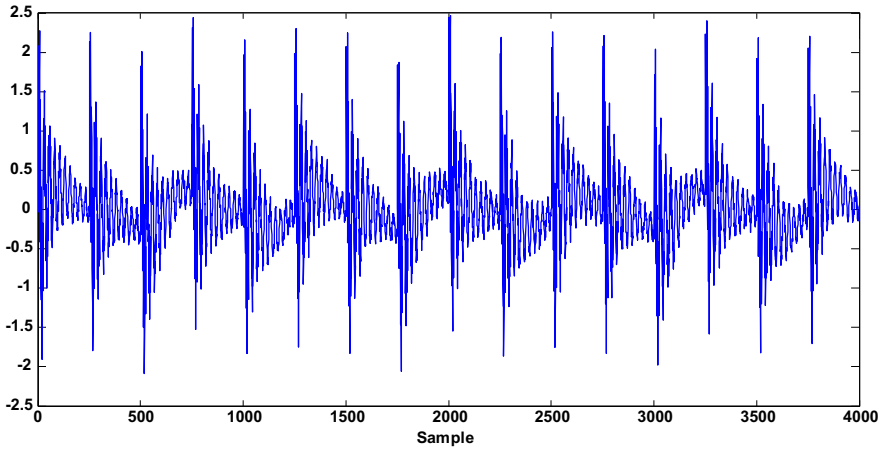

Fig. 6. The simulated signal.

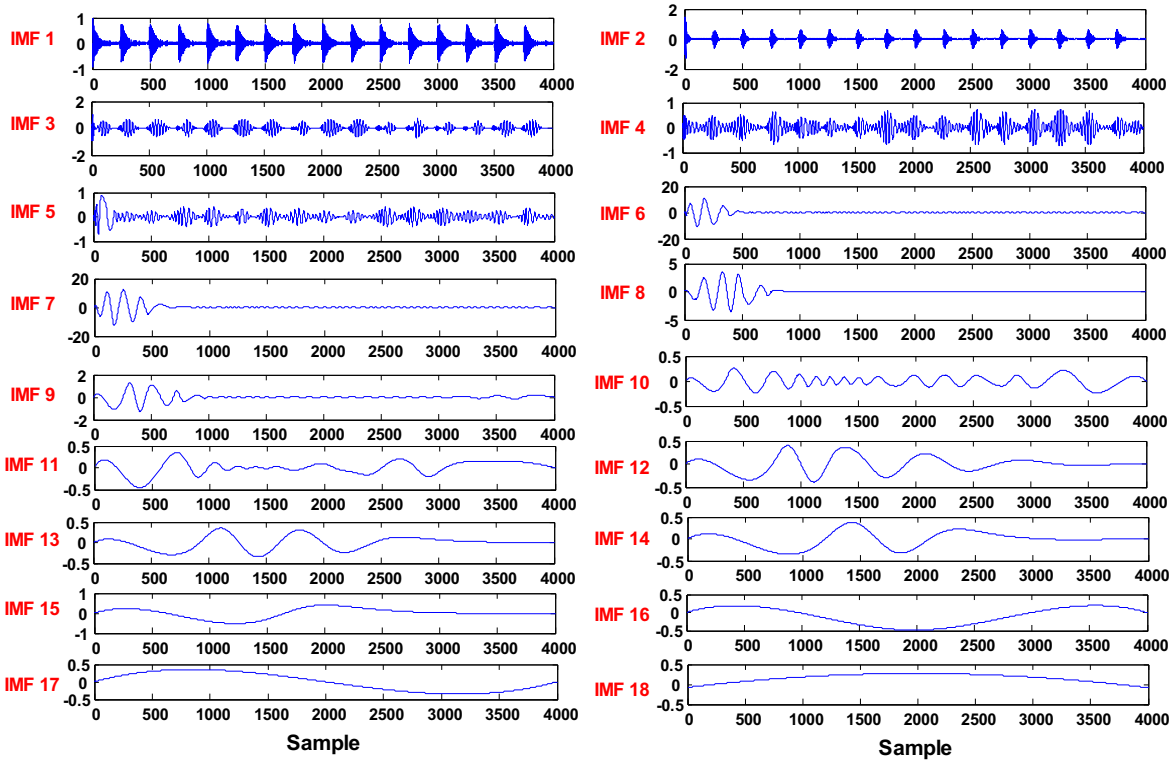

Fig. 7. The signal decomposition by EMD.

We detect an over estimation of the number of components ($N = 10$) with some meaningless false-components. Some mode mixing are obtained between IMF_2 and IMF_3. The second and third resonance frequencies are in the same IMF_2. Also a mode mixing is observed between IMF_3, IMF_4 and IMF_5.

3.1.2. *Application of EWT*

The segmentation of spectrum, as presented by Gilles [12], can estimate the different modes when the signal is composed as a sinusoidal waveform. However, for a complex signal like it is for a bearing signal as presented by Eq. (13), a separation of modes is difficult. The main problem is due to the fact that a bearing defect generates modulation frequencies and the algorithm, as presented, considers the modulation as an interested mode. For this reason, we propose to increase the frequency resolution to mask the modulation, by reducing the time of acquisition. The better way to do this is to take only one shock that excite the natural frequencies as shown in Fig. 10, and not consider the repetitive signal.

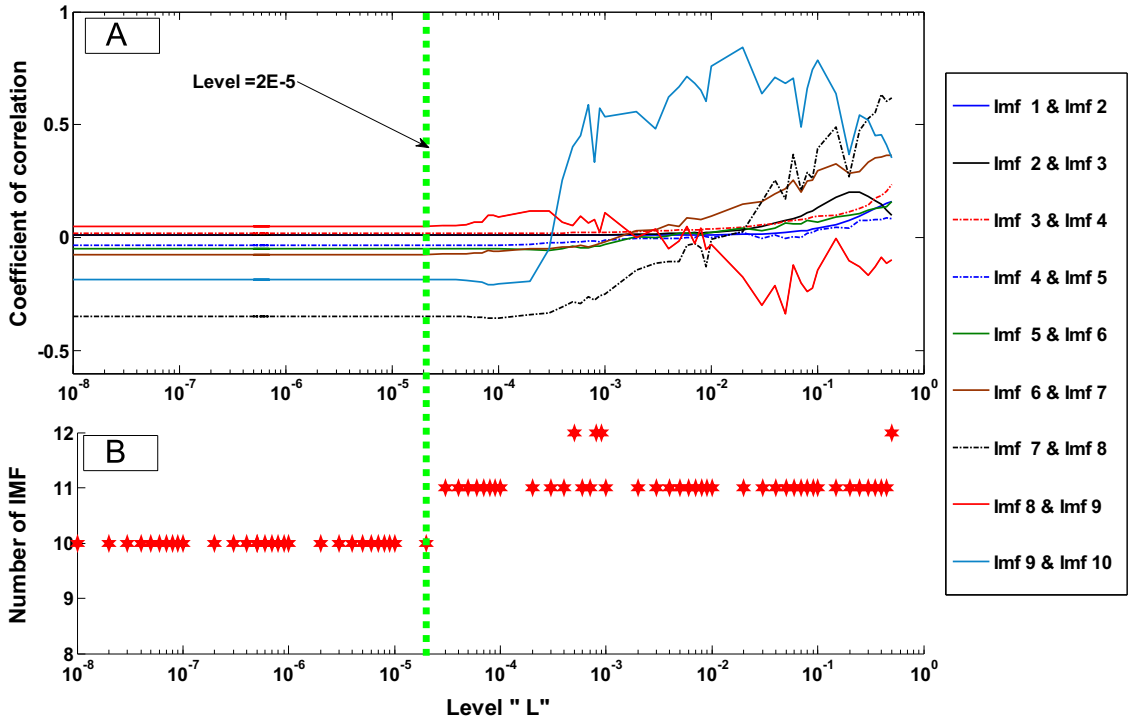

Fig. 8. (A) The correlation coefficient between successive IMF and (B) the number of IMF computed by EEMD.

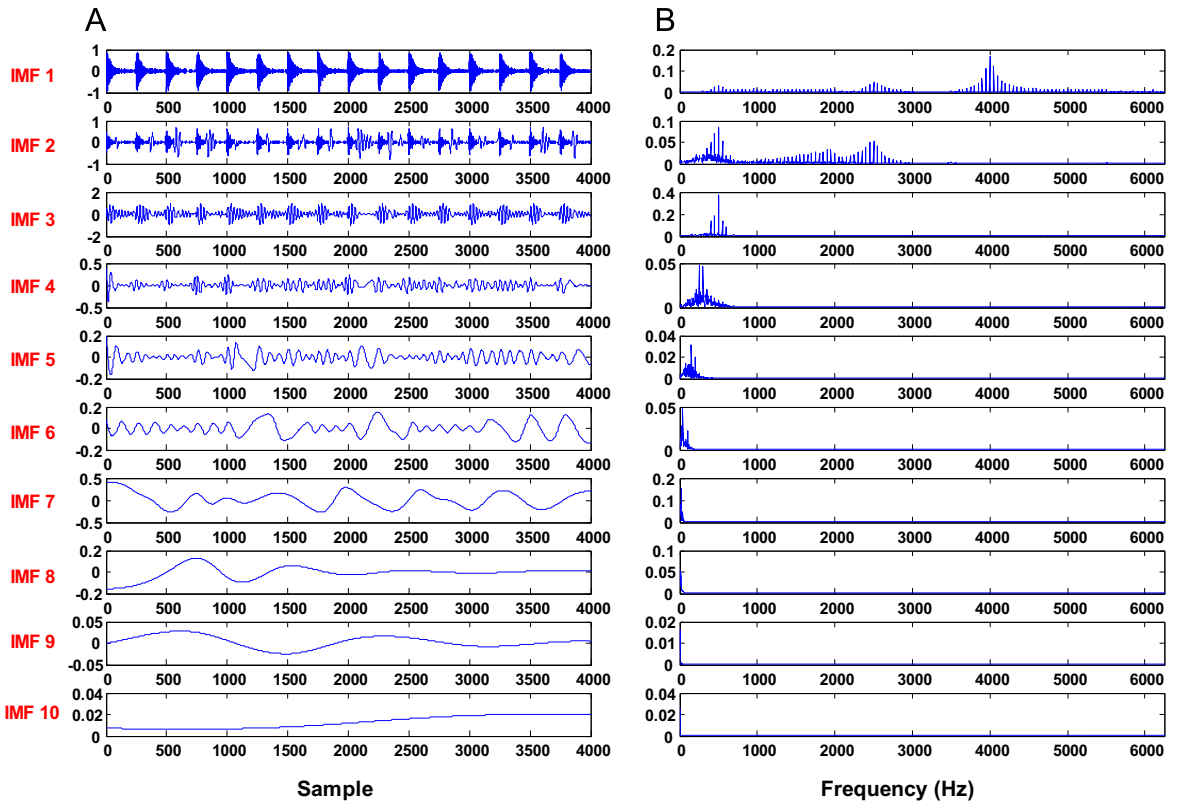

Fig. 9. (A) The decomposition EEMD of the signal and (B) the spectrum of each*IMF*.

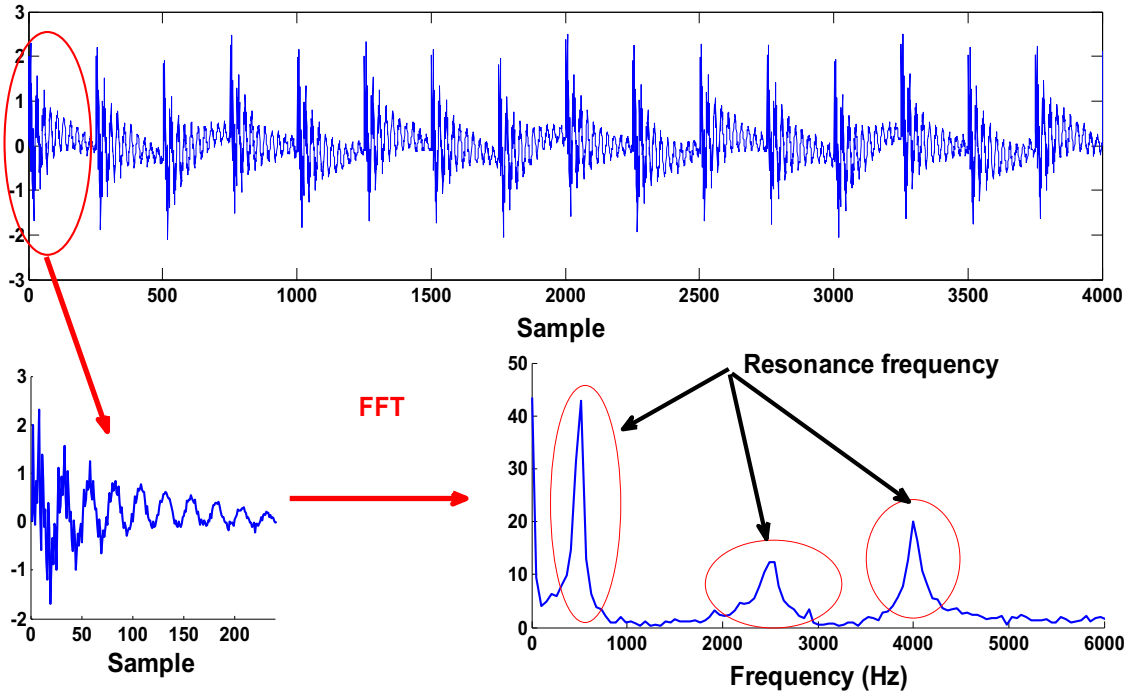

Fig. 10. The segmentation of the spectrum before computing the filter bank.

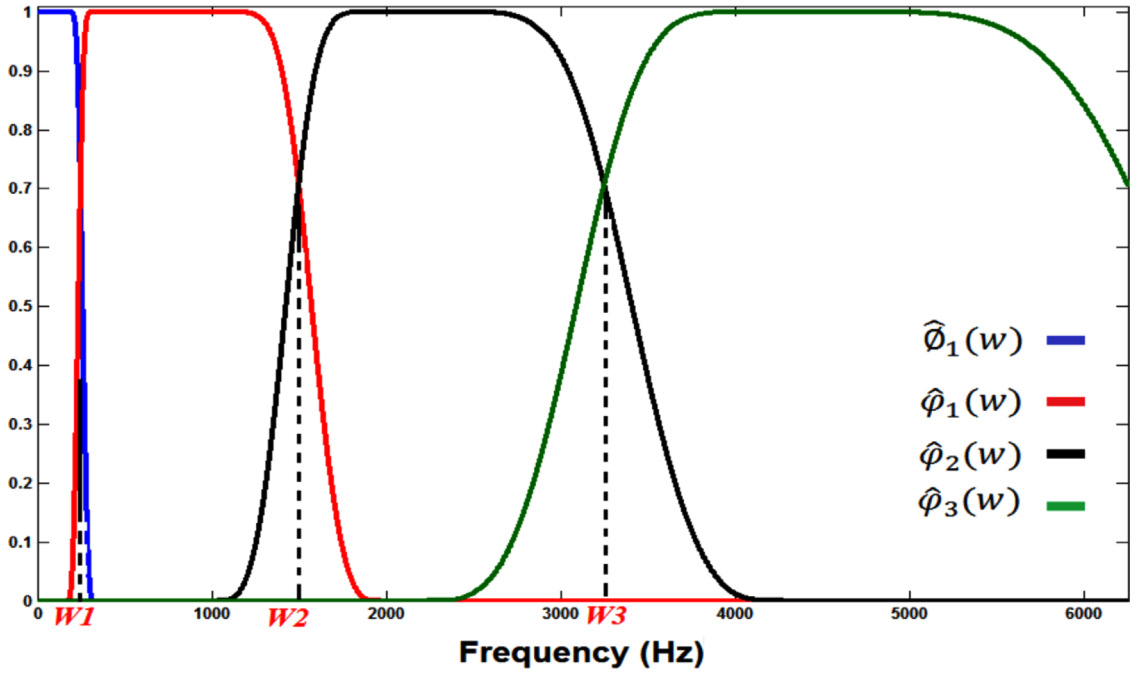

Fig. 11. Fourier partitioning of the empirical filter bank, $\hat{\phi}_1(w)$scaling function, $\hat{\varphi}_n(w)$empirical wavelet.

Fig. 11 shows the Fourier partitioning of the estimated empirical filter bank. $\hat{\phi}_1(w)$is the scaling function, $\hat{\varphi}_n(w)$ $(n=1..3)$ is the empirical wavelet, with $W1=250$ Hz, $W3=3250$ Hz (including 0 and $F_s/2$) are the boundaries support of the filter bank. Applying this filter bank to the signal, the decomposition is shown in Fig. 12. Fig. 12(A) and (B) shows the EWT of the signal $x(t)$ and the spectrum of each decomposition respectively. The authors observe that the EWT method can easily separate the components which correspond to each resonance frequency and harmonic frequencies and we note that there is no mode mixing.

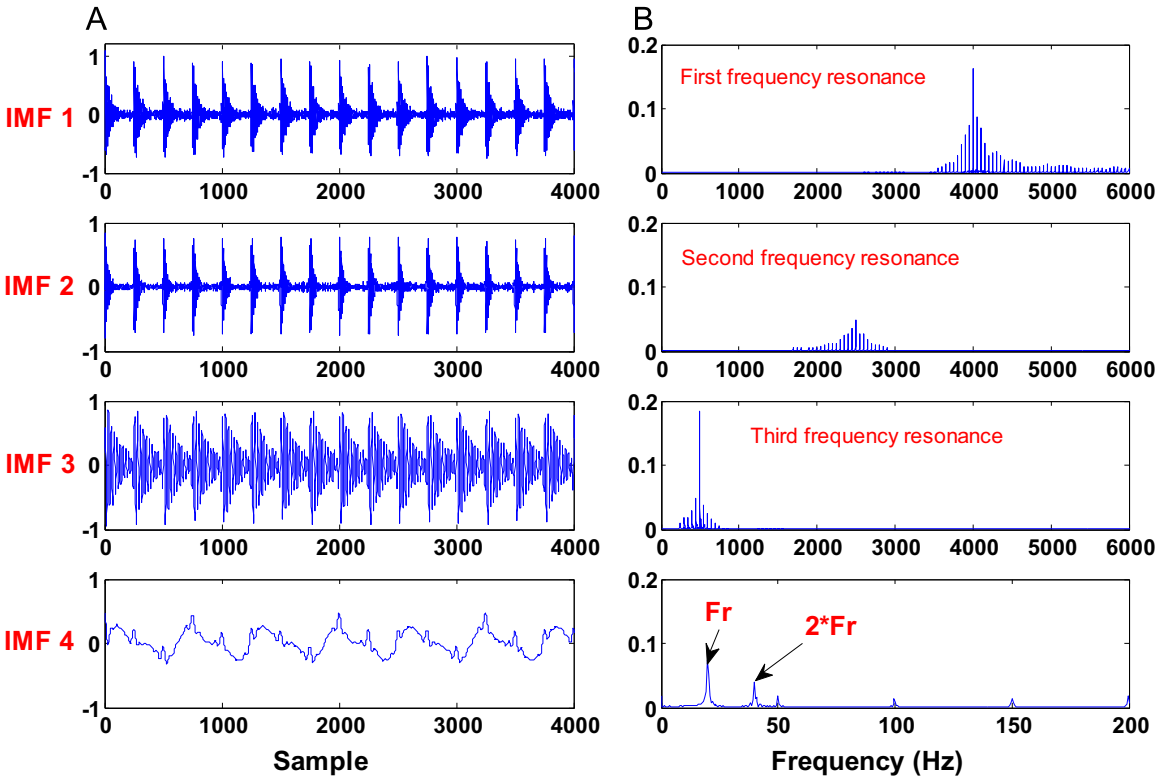

Fig. 12. (A) The decomposition EWT of the signal and (B) the spectrum of each*IMF*.

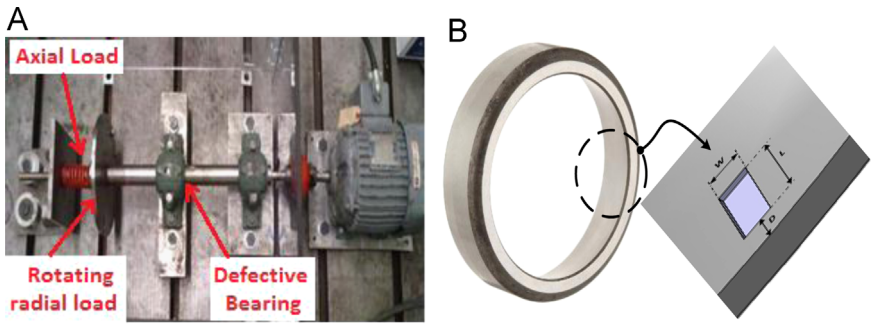

Fig. 13. (A) The test bench and (B) the defect on the outer race.

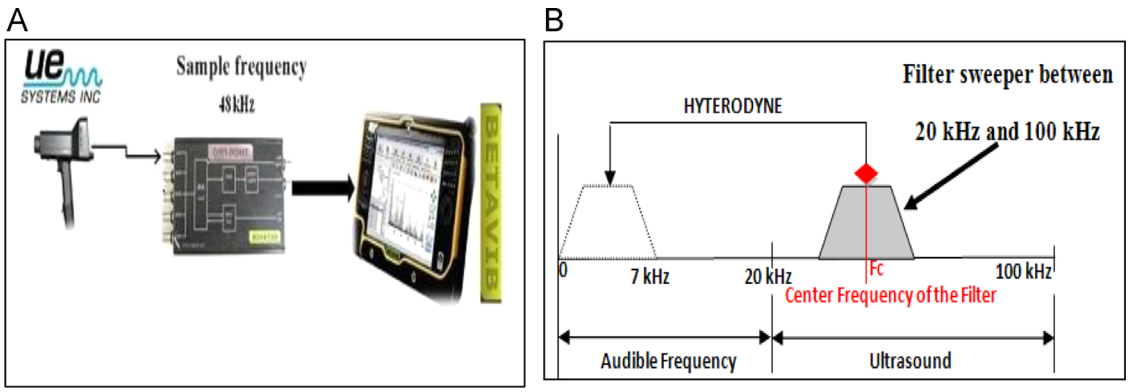

Fig. 14. (A) Data acquisition system and (B) heterodyne principle (ref: UE system).

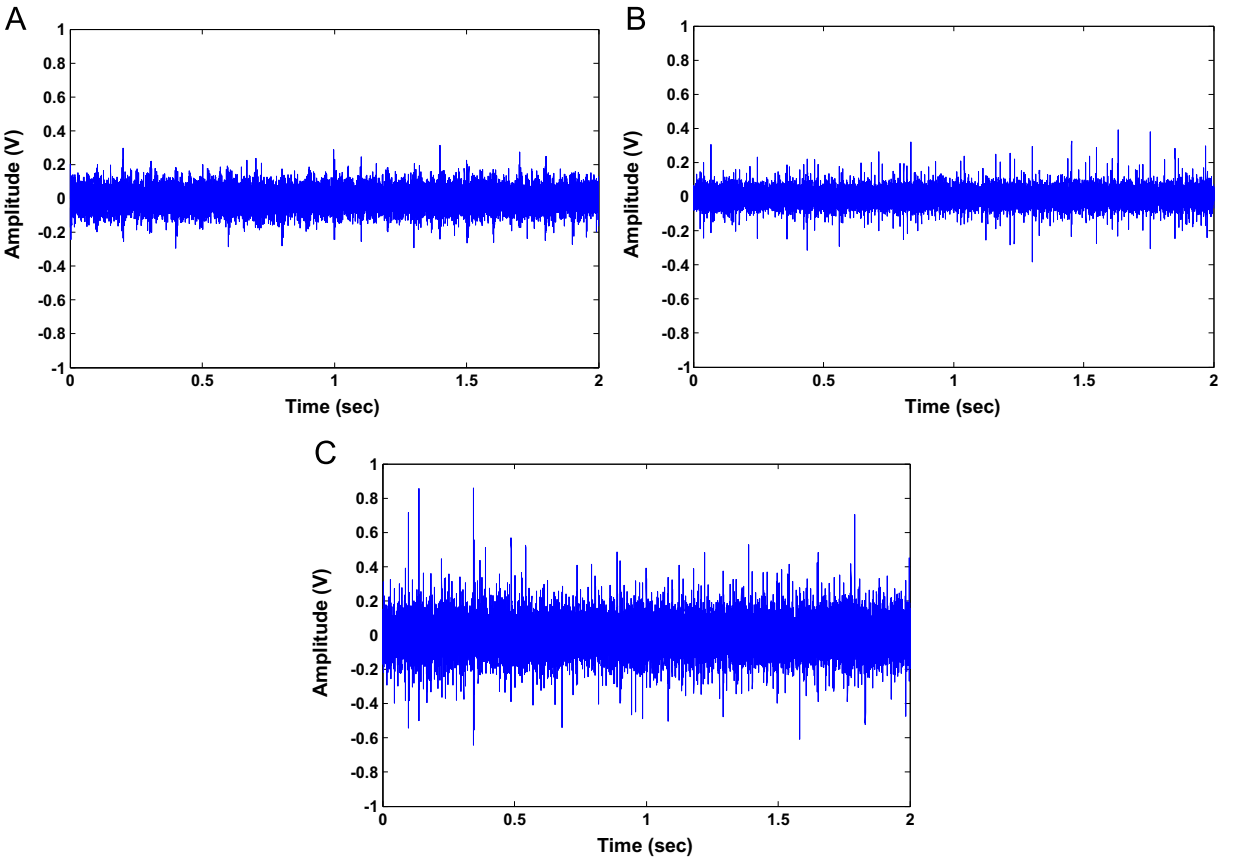

Fig. 15. Temporal signal: (A) Healthy bearing, (B) defect 50 μm, and (C) defect 100 μm.

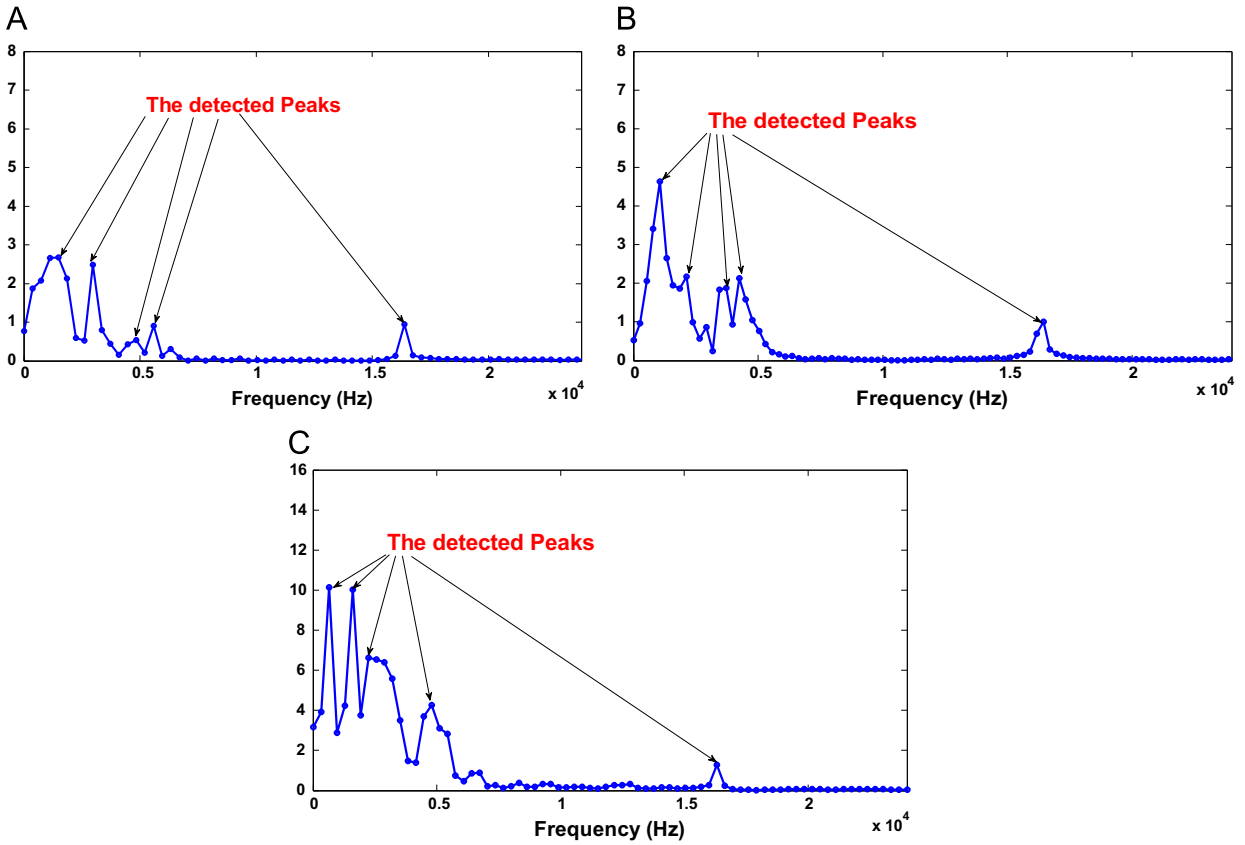

Fig. 16. The segmentation of the spectrum by using the same methodology described in Fig. 10: (A) Healthy, (B) defect 50 μm, and (C) defect 100 μm.

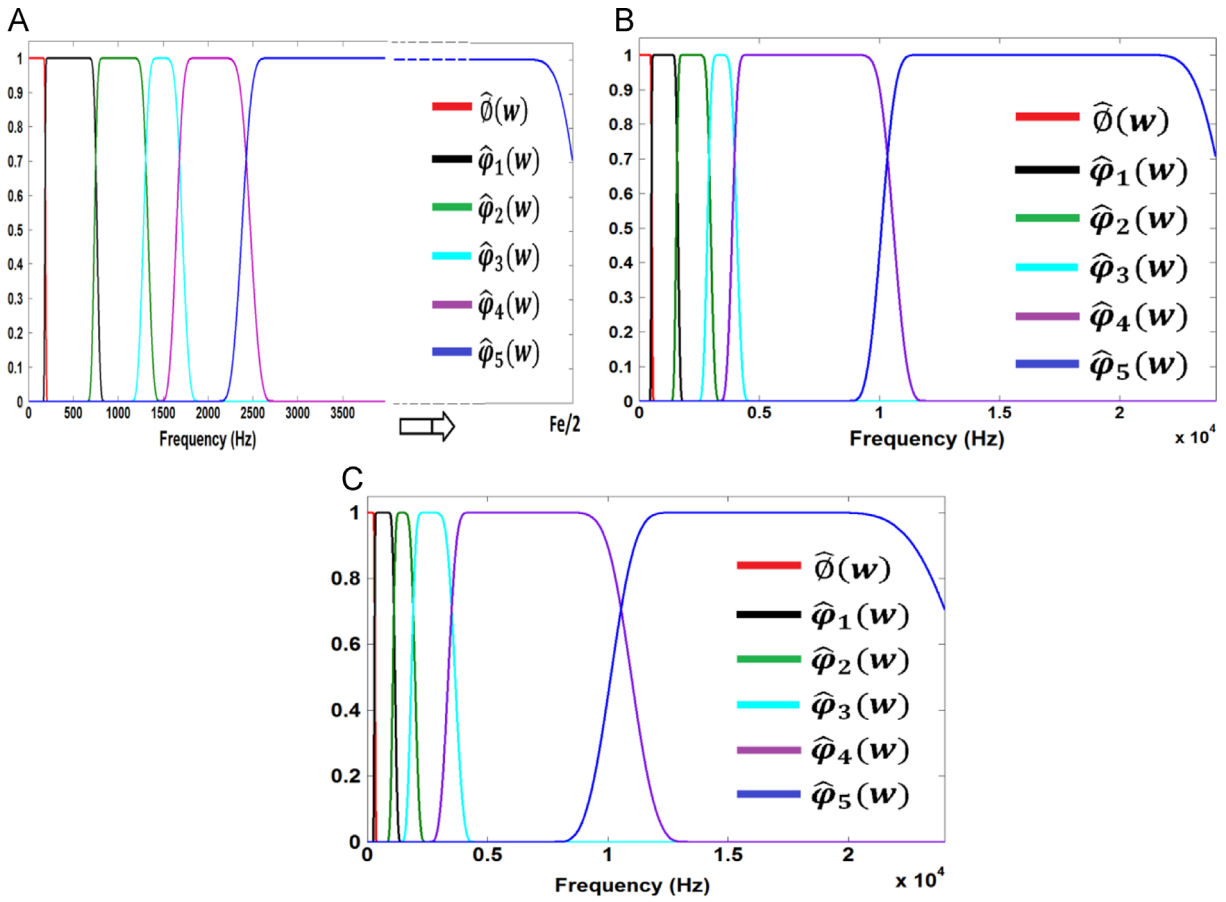

Fig. 17. Fourier partitioning of the empirical filter bank for acoustic emission signal, $\hat{\phi}_1(w)$scaling function, $\hat{\varphi}_n(w)$empirical wavelet: (A) Healthy bearing, (B) defect 50 μm, and (C) defect 100 μm.

In conclusion, the results show that when a signal is simple like the first simulation signal as in the preceding section, the performance of EEMD is similar to EWT, except for the time computation. However, when the signal is complex, like a model of bearings as presented in this section, the EEMD stays ever better than the EMD but present a lot of problems which are related to the estimation of the number of modes and mode mixing. EWT gives always the expected results after the number of modes has been identified.

3.2. Experimental application to bearing defect diagnosis

3.2.1. Experimental setup

The test bench used in this study is shown in Fig. 13(A) shaft is supported by two bearings and connected to a motor with a flanged coupling bolted rubber. Three systems were investigated, one with a healthy bearing (D0) and the two others with artificially defects (on the outer race) of different size. The defected bearing has a groove on the outer race as shown in Fig. 13(B). The localized defects were created on the outer race by using an Electric Discharge Machine (EMD) to keep their size and depth under control. The size of the artificial defect was about 200 μm in depth and the width (W) of the groove was 50 μm for the first defect (D1) and 100 μm for the second one (D2).

The equipment acoustic emission [30] is shown in Fig. 14(A). They consist in an ultrasound detector (UE Systems UltraProb 10,000). The sensor is connected to an analog digital converter (THOR Analyzer PRO: DT9837-13310) with a sampling frequency of 48 kHz. The latter is connected to a collector-analyzer BETAVIB. The ultrasonic sensor used in this study operates in the lower ultrasonic spectrum from 20 kHz to 100 kHz. A heterodyne circuit converts this high frequency acoustic emission signal filtered around a central frequency Fc into an audible signal (0–7 kHz) (Fig. 14(B)). The heterodyned signal may then be recorded through conventional data acquisition systems at 48 kHz. The mechanical system is excited by an unbalance mass rotating. The signals from the healthy bearing (D0) and the two bearings (D1 and D2) were recorded when rotating at a speed of 600 rpm.

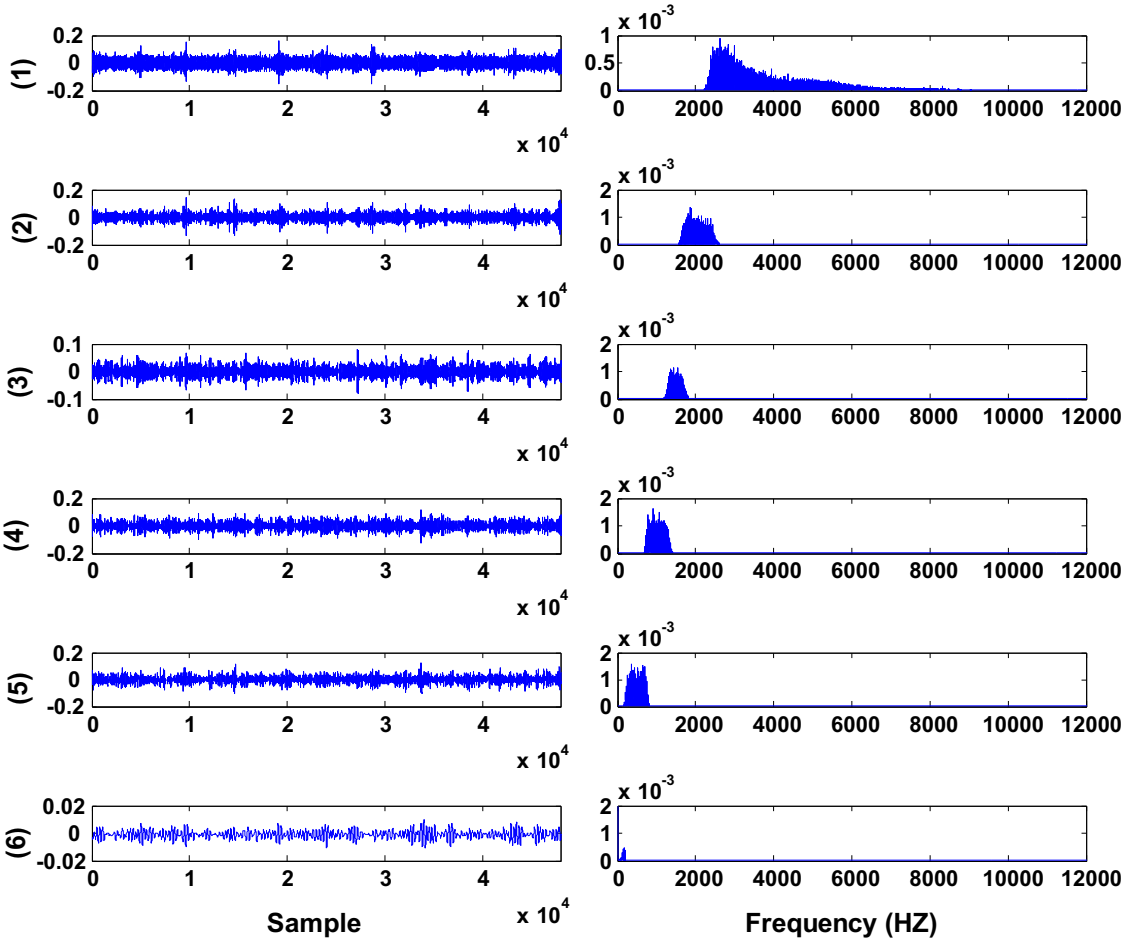

Fig. 18. EWT decomposition of acoustic emission of the healthy bearing.

3.2.2. Experimental application

The EWT method was experimentally applied to the acoustic emission data. Fig. 15 shows the temporal signal of the data acquired. The same procedure, described in Fig. 10, is used to decompose each signal. The better way to get a good segmentation is to take only a part of the signal to compute the spectrum. The ideal case is to choose one shock. The number of the simple used to compute the spectrum before the segmentation is 128 samples. The spectrums are presented in Fig. 16. According to these spectrums, globally, 5 peaks can be distinguished which can be used for computing the support of the filter bank. So, the support boundaries of the filter bank are defined as the middle between successive frequencies associated with these peaks, including the 0 and $F_s/2$.

Fig.17(A), (B) and (C), shows the Fourier partitioning of the estimated empirical filter bank ($\hat{\phi}_1(w)$ is the scaling function, $\hat{\varphi}_n(w)$ $(n=1..5)$ is the empirical wavelet) for the healthy bearing, the defect D1 and the defect D2, respectively. Applying those filters to its respective signal, a series of IMF are obtained. Figs. 18, 19 and 20 show the six *IMFs* of the EWT decomposition for the healthy bearing, the defect D1 and the defect D2, respectively. It may be noticed that for the defect D1 a repetitive impulse are located in the second IMF and are more perceptible when the defect growth (D2). For the other *IMFs*, the impulses are hidden in the noise. In case of the healthy bearing, quasi-random shocks signals are observed. This, in fact, reveals a slight defect, which can be of geometric origin, such as the rings or ball roundness.

The envelope spectral analysis based on the Hilbert Transform has proven to be a good tool for the diagnosis of local faults in rolling bearings. It extracts the characteristic defect frequencies of faulty bearings along with the modulation so that the type of defect can be determined. In the following steps, a bearing fault diagnosis is conducted on the selected *IMFs*, i.e.: the resultant signals obtained using the EWT method, to verify their features in the frequency domain.

3.2.3. Selection of IMF

After performing EWT on a signal, we obtain a series of *IMFs*. Some of these *IMFs* are closely related to faults of bearing, but others just contain information useless for diagnosing the faults. Therefore, sensitive *IMFs* should be selected and irrelevant *IMFs* eliminated to construct a more accurate Hilbert–spectrum. At early stage of degradation of bearing, impulses

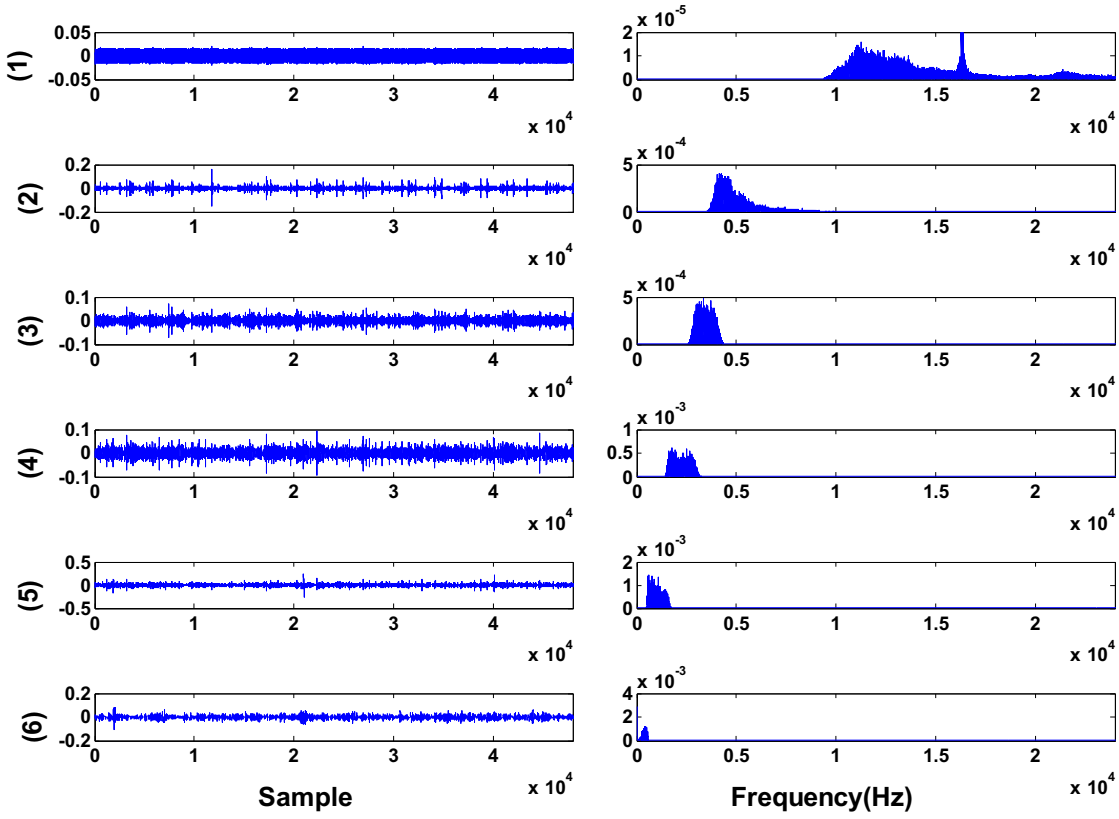

Fig. 19. EWT decomposition of acoustic emission signal (Defect 50 μm).

are created when a defect on a rolling surface impacts with another surface. The impulses are generated almost periodically. Tandon et al. [33] note that for an undamaged bearing, the kurtosis value is close to 3. A value greater than 3 is judged by itself to be an indication of damage. So, the kurtosis is a good way to characterise an impulsive signal [34–35]. The *Kurtosis* computed for raw signal and each *IMF* recorded from acoustic emission signals are shown in Tables 3 and 4 respectively.

A new method for developing an index based on *Kurtosis* is presented in order to select the more sensitive *IMF*as generated by EWT. The method compares the difference between the *Kurtosis* of each *IMF*of damaged and healthy bearing with the same difference based on the original signal (the acquired signal $x(t)$) (Eq. (16)). The *index_selection* is thus based on the difference between the amplitude distributions of the damaged and healthy bearings.

$$index\_selection = \frac{kurtosis(IMF_i)_{damaged} - kurtosis(IMF_i)_{Healthy}}{kurtosis(x)_{damaged} - kurtosis(x)_{Healthy}} \tag{16}$$

It may be noticed from Tables 3 and 4 that the *Kurtosis* of the healthy bearing (raw signal and *IMF*) is less than 5, as expected. This level could thus be used if the *Kurtosis* of the healthy bearing is unknown. Table 5 defines the criteria of selection. It indicates that an *IMF*will be selected of greater than 1.

The diagnosis procedure is well-described in Fig. 21. As presented in Fig. 21, we have two choices to perform the envelope spectrum:

1. Select the *IMF*with the higher *index_selection*
2. Select all the *IMFs* with *index_selection* greater than 1

Fig. 22 shows the envelope spectrum of the healthy bearing. Only the frequencies related to the shaft and its harmonics are detected.

Table 6 lists the values of *index_selection* for the acoustic emission signal. According to the *index_selection* listed in Table 6, IMF_2 exhibits the largest *index_selection* for both defects (D1 and D2). Figs. 23(A) and 24(A) highlight the envelope spectrum of acoustic emission when only analyzing IMF_2. Even when investigating a very small defect (D1), BPFO can be identified with its harmonic (Fig. 23(A)). Within the defect growth (D2) (Fig. 24(A)), a clear increase of the amplitude of the peaks related to BPFO and harmonics can be noticed.

A fault excites not only one mode, but the repetitive shocks generated by the defect at each revolution excite all the bearing harmonics and resonances. So when only one *IMF* is selected, even the best one, information that was included in

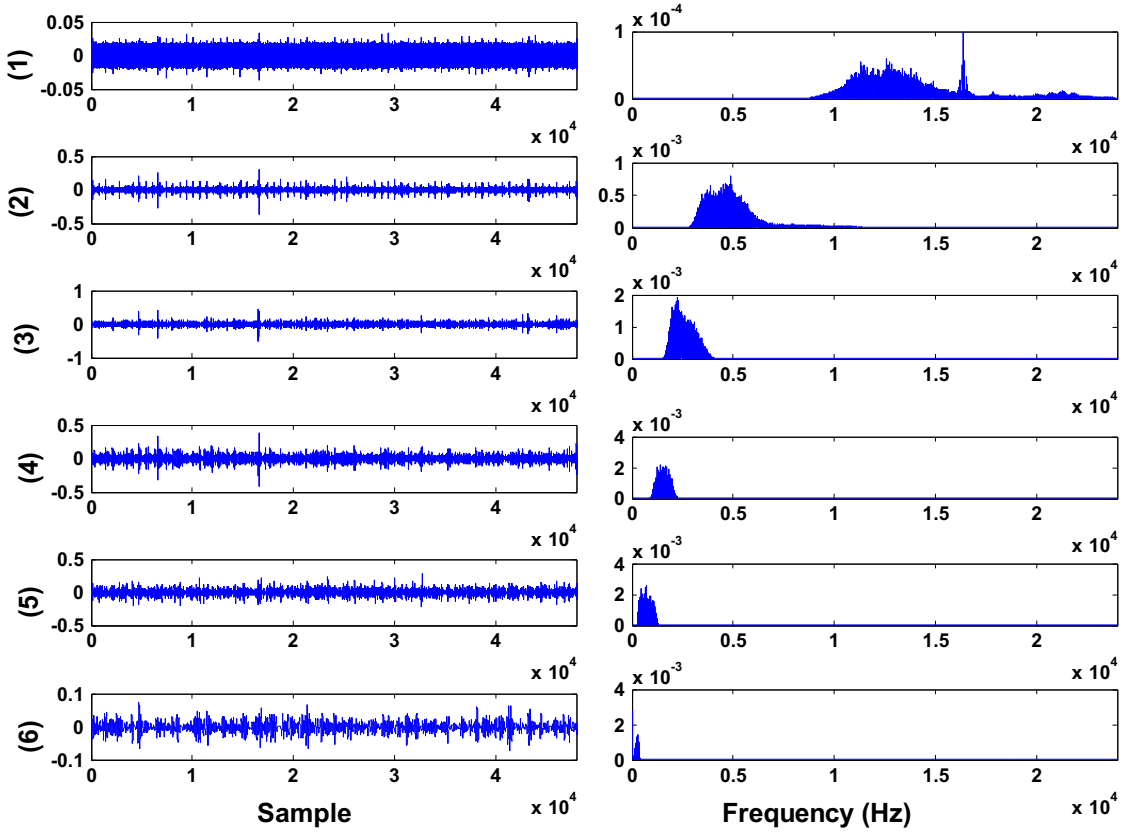

Fig. 20. EWT decomposition of acoustic emission signal (Defect 100 μm).

Table 3
Kurtosis values of the original signals for various faulty bearings.

	Kurtosis		
	healthy bearing	D1 = 50 μm	D2 = 100 μm
Acoustic emission	3.79	7.16	5.56

Table 4
Kurtosis values of each IMF for acoustic emission signals.

	IMF_1	IMF_2	IMF_3	IMF_4	IMF_5	IMF_6
Healthy bearing	3.82	4.97	3.34	3.27	3.61	3.18
D1 = 50 μm	1.51	17.68	8.32	7.55	7.59	4.42
D2 = 100 μm	1.64	12.31	5.75	4.78	4.21	3.74

Table 5
index_selection **criteria**

index_selection	Decision
< 1	The *IMF* is not selected
$= 1$	The difference between the distribution of amplitude of the both IMF (healthy & damaged) is the same as the raw signal (healthy & damaged)
> 1	The IMF is more impulsive than the raw signal. It is selected.

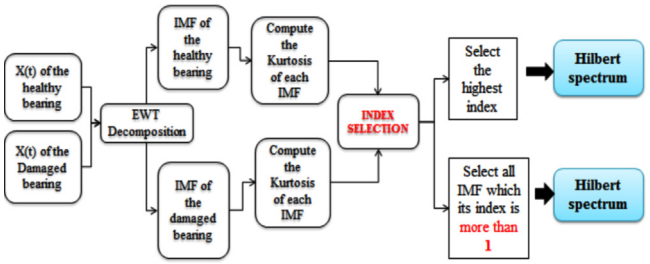

Fig. 21. Procedure for the selection of *IMF*.

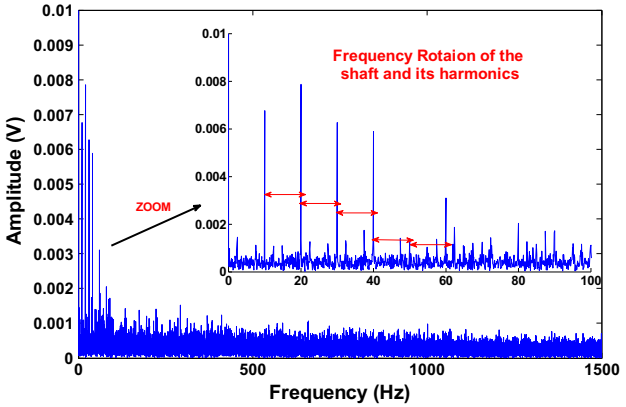

Fig. 22. Envelope spectrum of acoustic emission signal of the healthy bearing.

Table 6
The *index_selection* **of acoustic emission signal**.

	IMF_1	IMF_2	IMF_3	IMF_4	IMF_5	IMF_6
D1 = 50 μm	−0.68	**3.77**	1.47	1.27	1.17	0.36
D2 = 100 μm	−1.23	**4.13**	1.35	0.85	0.33	0.31

other *IMFs* excited by the fault was lost. On the other hand, the key of the diagnostic is the amplitude of the BPFO and also the number of harmonics of the bearing frequencies [31,32]. Consequently, the method revealed to be more sensitive when choosing all the selected *IMF* excited by the fault. For this reason, we propose to select all the selected*IMFs* which present an *index_selection* greater than 1.

According to Table 6, the IMF_2, IMF_3, IMF_4 and IMF_5 were selected for a defect D1. The envelope spectrum of the sum of these *IMF* is presented in Fig. 23 (B). IMF_2 and IMF_3 were chosen for the defect D2. The envelope spectrum of the sum of these *IMF* is presented in Fig. 24(B). In the both cases, a growth of the amplitude of the BPFO and its harmonics compared to the same case when only using the IMF_2 with the highest *index_selection* is noted (Figs. 23(A) and 24(A)). So, this confirms that the information related to the defects is not only included in one *IMF* but other *IMFs* are also excited by the defect.

4. Conclusions

In this paper, a recent approach, called Empirical Wavelet Transform (EWT) for fault diagnosis of bearings is investigated. A comparison between EWT, EMD and EEMD is made by using a numerically simulated signal. This study allowed us for improving the EEMD method by developing a method for choosing the appropriate amplitude of the added noise. It was noticed that EMD always overestimates the number of modes. EEMD gives the same results than EWT by choosing the suitable noise. However, the results shown that EWT, compared to EMD and EEMD, could reduce the time computation. EMD, EEMD and EWT method were applied to a numerical signal reflecting the behavior of damaged bearings; the results shown the effectiveness of EWT to decompose a signal unlike EEMD which overestimates the number of components and meaningless false-components obtained. The EWT method has then been applied to experimental signals obtained by acoustic emissions measurements. An index based on *Kurtosis* was developed for selecting the *IMF* more sensitive to the

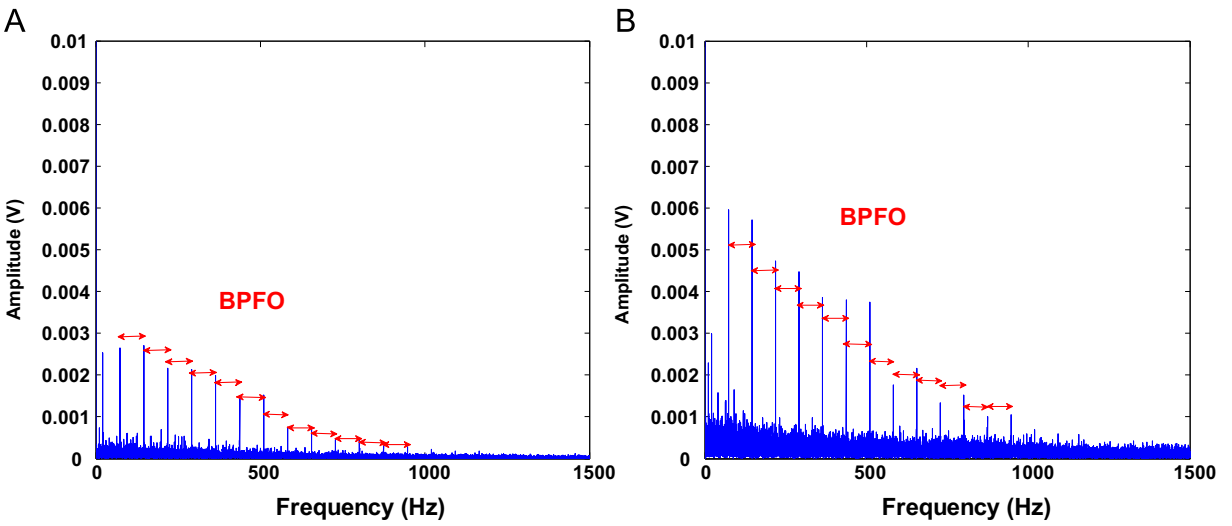

Fig. 23. Envelope spectrum of acoustic emission signal of the defect D1 (A) *IMF* with the highest *index_selection* and (B) all *IMF* with *index_selection* greater than 1.

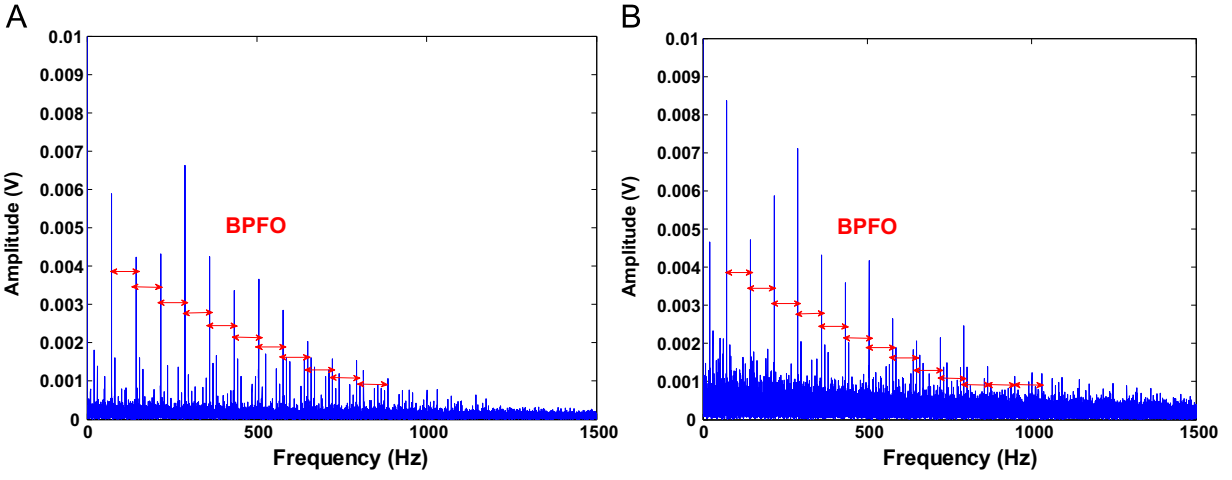

Fig. 24. Envelope spectrum of acoustic emission signal of the defect D2 (A) *IMF* with the highest *index_selection* and (B) all *IMF* with *index_selection* greater than 1.

defect. The results reveal that choosing all the selected *IMF* was more efficient than choosing the best one. The results have shown that the EWT method can effectively reveal the frequency and associated harmonics of the faulty bearing.

Acknowledgments

The support of NSERC (Natural Sciences and Engineering Research Council of Canada), FQRNT (Fonds Québecois de la Recherche sur la Nature et les Technologies), MITACS Canada and Pratt & Whitney Canada is gratefully acknowledged.

Appendix A. : Empirical Wavelet Transform

The filter bank is defined by the empirical scaling function and the empirical wavelets given by the expressions of (1) and (2), respectively.

$$\hat{\phi}_n(w) = \begin{cases} 1 & \text{if } |w| \le (1-\gamma)w_n \\ \cos\left[\frac{\pi}{2}\beta\left(\frac{1}{2\gamma w_n}(|w|-(1-\gamma)w_n)\right)\right] & \text{if } (1-\gamma)w_n \le |w| \le (1+\gamma)w_n \\ 0 & \text{otherwise} \end{cases} \quad (1)$$

$$\hat{\varphi}_n(w)=\begin{cases}1 & \text{if } (1+\gamma)w_n \le |w| \le (1-\gamma)w_{n+1}\\ \cos\left[\frac{\pi}{2}\beta\left(\frac{1}{2\gamma w_{n+1}}(|w|-(1-\gamma)w_{n+1})\right)\right] & \\ & \text{if } (1-\gamma)w_{n+1} \le |w| \le (1+\gamma)w_{n+1}\\ \sin\left[\frac{\pi}{2}\beta\left(\frac{1}{2\gamma w_n}(|w|-(1-\gamma)w_n)\right)\right] & \\ & \text{if } (1-\gamma)w_n \le |w| \le (1+\gamma)w_n\\ 0 & \text{otherwise}\end{cases} \tag{2}$$

The function $\beta(x)$ is an arbitrary $C^k([0\ ,1])$function defined as:

$$\beta(x)=\begin{cases}0 & \text{if } x\le 0\\ \text{and } \beta(x)+\beta(1-x)=1\ \forall x\in[0,\ 1] & \\ 1 & \text{if } x\ge 1\end{cases} \tag{3}$$

Many functions satisfy these properties, the most used in the literature [30] is:

$$\beta(x)=x^4(35-84x+70x^2-20x^3) \tag{4}$$

And γ is chosen by Eq. (5)

$$\gamma<\min_n\left(\frac{w_{n+1}-w_n}{w_{n+1}+w_n}\right) \tag{5}$$

Using (Eqs. (1) and 2), the reconstruction of the signal is obtained by:
The detail coefficients are given by the inner products with the empirical wavelets $\hat{\varphi}_n$:

$$IMF_{n=1:N-1}=W_x(n,t)=\langle x(t),\hat{\varphi}_n\rangle=IFFT\left(X(w)\times\hat{\varphi}_n(w)\right) \tag{6}$$

The approximation coefficients are given by the inner product with the scaling function $\hat{\phi}_1$:

$$IMF_N=W_x(1,t)=\left\langle x(t),\hat{\phi}_1\right\rangle=IFFT\left(X(w)\times\hat{\phi}_1(w)\right) \tag{7}$$

References

[1] N.E. Huang, Z. Shen, S.R. Long, The empirical mode decomposition and the Hilbert spectrum for nonlinear and non-stationary time series analysis, Proc. R. Soc. Lond. 454 (1998) 903–995.
[2] M. Kedadouche, M. Thomas, A. Tahan, Empirical mode decomposition of acoustic emission for early detection of bearing defects, in: Proceedings of the 3rd International Conference on Condition Monitoring of Machinery in Non-Stationary Operations (CMMNO), Ferrara (It), 9 May, 2013, 11pp.
[3] Y.G. Lei, J. Lin, Z.J. He, M.J. Zuo, A review on empirical mode decomposition in fault diagnosis of rotating machinery, Mech. Syst. Signal Process. 35 (1–2) (2013) 108–126.
[4] Z.H. Wu, N.E. Huang, Ensemble empirical mode decomposition: a noise assisted data analysis method, Adv. Adapt. Data Anal. (2009) 11–14.
[5] Xia Wang, Changwen Liu, Fengrong Bi, Xiaoyang Bi, Kang Shao, Fault diagnosis of diesel engine based on adaptive wavelet packets and EEMD-fractal dimension, Mech. Syst. Signal Process. 41 (2013) 581–597.
[6] Zhipeng Feng, Ming Liang, Yi Zhang, Shumin Hou, Fault diagnosis for wind turbine planetary gearboxes via demodulation analysis based on ensemble empirical mode decomposition and energy separation, Renew. Energy 47 (2012) 112–126.
[7] Jinshan Lin, Improved ensemble empirical mode decomposition and its applications to gearbox fault signal processing No. 2, IJCSI Int. J. Comput. Sci. 9 (6) . ISSN: 1694-0814.
[8] Peter W. Wei Guo, Tse, Alexandar Djordjevich, Faulty bearing signal recovery from large noise using a hybrid method based on spectral kurtosis and ensemble empirical mode decomposition, Measurement 45 (2012) 1308–1322.
[9] Changqing Shen, Fei Hu, Zhongkui Zhu, Fanrang Kong, Rolling bearing fault degree recognition based on ensemble empirical mode decomposition and support vector regression, Appl. Mech. Mater. 333–335 (2013) 550–554.
[10] L.V. Zhongliang, A.N. Peiwen, Baoping Tang, Lihui Zhang, The application of EEMD to fault diagnosis of rolling bearing, Adv. Mater. Res. 765–767 (2013) 2065–2069.
[11] T.Y. Wu, Y.L. Chung, Misalignment diagnosis of rotating machinery through vibration analysis via the hybrid EEMD and EMD approach, Smart Mater. Struct. 18 (095004) (2009) 13.
[12] J. Gilles, empirical wavelet transform, IEEE Trans. signal Process. 61 (16) .
[13] Q. Liu, F. Chen, Z. Zhou, Q. Wei, Fault diagnosis of rolling bearing based on wavelet package transform and EEMD, Adv. Mech. Eng. Hindawi 2013 (2013) 6792584.
[14] M. Kedadouche, M. Thomas, A. Tahan, Monitoring machines by using a hybrid method combining MED, EMD and TKEO, Adv. Acoust. Vib. Hindawi 2014 (2014) 14592080.
[15] T.Y. Hou, Z. Shi, Adaptive data analysis via sparse time-frequency representation, Adv. Adapt. Data Anal. 2 (2011) 1–28.
[16] Norden E. Huang, Zheng Shen, Steven R. Long, Manli C. Wu, Hsing H. Shih, Quanan Zheng, Nai-Chyuan Yen, Chi Chao Tung, Henry H. Liu, The empirical mode decomposition and the Hilbert spectrum for nonlinear and non-stationary time series analysis, R. Soc. Proc. Math. Phys. Eng. Sci. 454 (1971) (1998) 903–995.
[17] Y. Lei, M.J. Zuo, Fault diagnosis of rotating machinery using an improved HHT based on EEMD and sensitive IMFs, Meas. Sci. Technol. 20 (2009) 125701–125712.
[18] Y. Lei, Z. He, Y. Zi, Application of the EEMD method to rotor fault diagnosis of rotating machinery, Mech. Syst. Signal Process. 23 (2009) 1327–1338.
[19] Y. Lei, Z. He, Y. Zi, EEMD method and WNN for fault diagnosis of locomotive roller bearings, Expert Syst. Appl. 38 (2011) 7334–7341.
[20] T. Zhou, X. Tao, G. Mei, Jiang, N. Sun, Feed-axis gearbox condition monitoring using built-in position sensors and EEMD method, Robot. Comput. Integr. Manuf. 27 (2011) 785–793.
[21] W. Guo, P.W. Tse, Enhancing the ability of ensemble empirical mode decomposition in machine fault diagnosis, in: Proceedings of the Prognostics and System Health Management Conference, Macau, January 2010, pp. 1–7.

[22] M. Zvokelj, S. Zupan, I. Prebil, Multivariate and multiscale monitoring of large-size low-speed bearings using ensemble empirical mode decomposition method combined with principal component analysis, Mech. Syst. Signal Process. 24 (2010) 1049–1067.
[23] M. Zvokelj, S. Zupan, I. Prebil, Nonlinear multivariate and multiscale monitoring and signal denoising strategy using Kernel principal component analysis combined with ensemble empirical mode decomposition method, Mech. Syst. Signal Process. 25 (2011) 2631–2653.
[24] K.M. Chang, S.H. Liu, Gaussian noise filtering from ECG by Wiener filter and ensemble empirical mode decomposition, J. Signal Process. 64 (2011) 249–264.
[25] J. Zhang, R. Yan, R.X. Gao, Z. Feng, Performance enhancement of ensemble empirical mode decomposition, Mech. Syst. Signal Process. 24 (2010) 2104–2123.
[26] J.R. Yeh, J.S. Shieh, N.E. Huang, Complementary ensemble empirical mode decomposition: a novel noise enhanced data analysis method, Adv. Adapt. Data Anal. 2 (2010) 135–156.
[27] R.K. Niazy, C.F. Beckmann, J.M. Brady, S.M. Smith, Performance evaluation of ensemble empirical mode decomposition, Adv. Adapt. Data Anal. 1 (2009) 231–242.
[28] Wei Guo, P.W. Tse, A novel signal compression method based on optimal ensemble empirical mode decomposition for bearing vibration signals, J. Sound Vib. 332 (2) (2013) 423–441.
[29] Y.T. Sheen, A complex filter for vibration signal demodulation in bearing defect diagnosis, J. Sound. Vib. 276 (2004) 105–119.
[30] M. Kedadouche, M. Thomas, A. Tahan. Monitoring bearings by acoustic emission: a comparative study with vibration techniques for early detection. 30th seminar on machinery vibration CMVA, Niagara Falls (ON), 17 p., 25 Oct 2012.
[31] Thomas M., Masounave J., Dao T.M., Le Dinh C.T., Lafleur F. Rolling element bearing degradation and vibration signature relationship, 2nd international conference on surveillance methods and acoustical and vibratory diagnosis, SFM, Clamart, France, 1, pp. 267–277, 1995.
[32] M. Thomas, Reliability, predictive maintenance and machinery vibration (in french), PUQ, D3357, 2011, 633, ISBN 978-2-7605-3357-8.
[33] N. Tandon, A. Choudhury, A review of vibration and acoustic measurement methods for the detection of defects in rolling element bearings, Tribol. Int. 32 (1999) 469–480.
[34] N. Sawalhi, R.B. Randall., H. Endo, The enhancement of fault detection and diagnosis in rolling element bearings using minimum entropy deconvolution combined with spectral kurtosis, Mech. Syst. Signal Process. 21 (6) (2007) 2616–2633.
[35] H. Endo, R.B. Randall, Application of a minimum entropy deconvolution filter to enhance autoregressive model based gear tooth fault detection technique, Mech. Syst. Signal Process. J. 21 (2) (2007) 906–919.
[36] K. Thirumala, Estimation of single-phase and three-phase power-quality indices using empirical wavelet transform, IEEE Trans. Power Deliv. 30 (1) .